Radiation damage of the optical components of the ATLAS TileCal calorimeter at the High-Luminosity LHC

Beatriz Pereira[*]
Laboratory of Instrumentation and Experimental Particle Physics,
Av. Professor Gama Pinto 2, 1649-003 Lisboa Portugal

(Dated: February 3, 2021)

TileCal, a sampling hadronic calorimeter, is an essential component of the ATLAS detector at the LHC. The active material, made of plastic scintillating tiles, producing light when traversed by charged particles. The light is transmitted to photomultiplier tubes by wavelength shifting fibres.

The High Luminosity-LHC (HL-LHC) program will extend the TileCal lifetime for 20 years more than originally designed. The detector performance is affected by the increased exposure to radiation that will degrade the TileCal optics and by natural ageing. Since the TileCal's optical components cannot be replaced, their radiation hardness must be evaluated with precision. In addition, the experience gained with a real detector under harsh radiation conditions for long time will be invaluable for the design of future detectors at FCC or other detectors. The TileCal scintillators and fibres' response was determined by exploring information about dedicated calibration systems that employs a cesium source and laser light pulses. The uncertainties associated with the Laser calibration were studied to evaluate the optics' ageing. Run 2 data were analysed, indicating that cells of layer A, and B11 and C10 cells have already lost about 5% of light yield. No significant changes were found for the other cells. The results were extrapolated to the end of Run 3 and end of the HL-HLC, suggesting a light loss of about 20% for most cells, while the most irradiated may lose up to 80% of light yield. Nevertheless, the extrapolation uncertainty is large, so more data needs to be explored to reach better precision.

Keywords: LHC, ATLAS, TileCal, Radiation Hardness, Scintillator Detector

I. Introduction

Scintillator-based detectors are used to detect ionising particles in high energy physics, medical field and many applications of dosimetry. The scintillating materials used in the construction of these detectors may suffer damage, due to natural ageing of the materials, as well as with the accumulated radiation dose. A good knowledge of both is fundamental for the design of detectors of the future high energy experiments. The study of scintillator materials in search for increased radiation hardness is expected to have a boost in the near future in view of the upgrade European Strategy for Particle Physics, that remarked the importance of the R&D in preparation for the Future Circular Collider (FCC) [1]. The experienced gained with real detectors, such as those at the LHC, that are currently operating under harsh radiation damage conditions and for a long period of time will be paramount to guide the design of future detectors. The ATLAS experiment of the LHC is one example of a high energy physics experiment that uses plastic scintillator detectors in the Tile Calorimeter detector. The main purpose of this detector is to measure the energy and direction of hadrons and τ-jets by their interaction with the scintillator material, also contributing to the evaluation of the missing transverse energy. Scintillating light from TileCal is collected and guided by the wavelength shifting fibres until it reaches the photomultiplier tube and read-out electronics.

The main subject of this work is to study the radiation hardness of the TileCal optical components with a two-fold motivation. On the one hand, the TileCal detector was designed to operate for a period of up to six years at a maximum instantaneous $p-p$ collisions luminosity of 10^{34} cm^{-2} s^{-1}. The extension of the LHC programme with a phase of High Luminosity (HL-LHC) that will last for longer than 10 years more, operating at an instantaneous luminosity of 5 to 7 times larger than the design, will challenge the detector components that cannot easily be exchanged and that have to operate with good performance till the end of the LHC lifetime. This is the case of the scintillating and optical components of the TileCal. It is, thus, crucial to estimate their expected radiation damage at the end of the HL-LHC phase, in order to design strategies to mitigate or recover at least part of the performance loss, in case it is found to be severe. On the other hand, the measurements of radiation hardness with a real detector that has operated up to now for more than 10 years, will be invaluable for the design of future detectors since some of the effects (such as low radiation doses for very long periods of time) are not easy to simulate in laboratory conditions or beam tests.

To study the radiation damage of the TileCal optical components, it is important to understand the uncertainties associated with the TileCal calibration procedures since they will limit the precision on the measurement of the radiation damage. Part of the work was dedicated to determine the uncertainties associated to the Laser system.

The LHC Run 2 ended in 2018, and Run 2 data was used to measure the light yield of the TileCal optics during this Run. These measurements were modelled as a function of the simulated dose in Run 2 and extrapolated to future runs in order to study the radiation hardness of the optical components at the end of the Run 3 and HL-LHC phase, the material recovery was not taking into account.

---

[*] beatrizcpereira@tecnico.ulisboa.pt

II. Scintillator Detectors

When ionising radiation interacts with matter, it loses energy by transmitting it to the material. The electrons in scintillating materials will be excited when interacting with ionising radiation and the release of photons, with smaller energy than the initial incident radiation, will occur upon de-excitation. This phenomenon is called scintillation. Larger ionization energy will generate more photons.

Scintillating materials can be separated into two broad classes: organic an inorganic. Organic materials are cheap, have a good time response and light output and can be easily shaped. A typical organic scintillator is composed of three parts: a polymer base, a primary dopant and a secondary dopant. The absorption and emission wavelenghts of each of these components suffers a shift, allowing the wavelenght emitted by the secondary dopant to be compatible with the light detection of the photodetector.

However, organic materials are known to suffer from radiation damage and the light output of the scintillator decreases exponentially with the dose defined as the energy deposited, E_{dep}, by ionising radiation per unit mass of the material:

$$d = \frac{E_{dep}}{m} = \frac{E_{dep}}{\rho \times volume} \tag{1}$$

where m is the material mass and ρ the density of the material. The scintillating material's molecule chains suffer damage when exposed to radiation, breaking and cross-linking. This leads to changes in the structure of the polymers and the production of free radicals, which absorb and scatter the scintillation light affecting the light yield, transmittance and mechanical properties of scintillators [2]. The constant values of the exponential depends mainly on the material used, but some studies also showed a dependency on the dose rate. The dose rate effects are visible in Figure 1, where the light output for scintillators employed in the CMS detector at the LHC accelerator as a function of the integrated luminosity, a quantity proportional to the dose is shown for different scintillators. Their dose rates span 4 orders of magnitude if the constant values of the exponential does not depend on the dose rate, it will be expected that the scintillating tiles have the same exponential constants. In Figure 1 this values is not the same implying that scintillating tiles with a smaller exponential constant suffer more damage for the same dose than the tiles with higher exponential constants.

The dose rate effects can be related to gas diffusion in the surrounding atmosphere into the irradiated object. For example, if this gas is oxygen, the ionisation of this molecule may lead to the formation of free radicals, which can induce the breaking of the polymer chain. The diffusion is a slow process, therefore if the dose rate is very high, the impact of the total absorbed dose will be smaller than in the case of long irradiation at a low dose rate [3].

In summary, to obtain the minimum radiation damage, the based material should be chosen according to the detector's environment components, and the concentrations of the dopants should be chosen to maximise the efficiency of the wavelength shift. The work presented on this dissertation studies the radiation hardness of the plastic scintillators used in the Tile Calorimeter of the ATLAS detector at the LHC. These are based on polystyrene (PS) and doped with a primary dopant with a concentration of 1.5% p-terphenyl (PTP) and with a concentration of 0.044% 4-bis(5-phenyl-2-oxazolyl)benzene (POPOP) for the secondary dopant [4].

The last component of a scintillator detector is a photodetector, such as a photomultiplier tube (PMT). The PMT is govern by the photoelectric effect for converting light into electrical signal. The conversion efficiency of the device must be high to maximize the collected information in the form of light to the output information in form of electrical signal. The typical efficiency of a PMT is of the order of 30% [5].

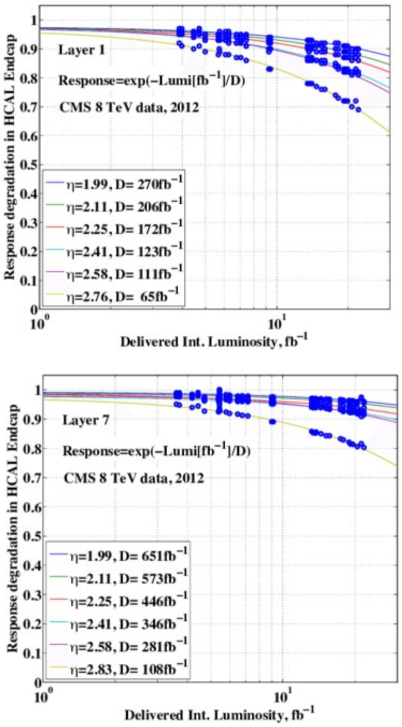

Figure 1. Relative light output for CMS tiles as a function of integrated luminosity for (top) the layer 1 and (bottom) layer 7. D is the exponential constant governing the degradation rate [6].

III. The ATLAS Experiment at CERN's Large Hadron Collider

The LHC is an accelerator located in the European Organization for Nuclear Research - CERN - facilities near Geneva. CERN's mission is to understand the birth of our universe, how the universe works, and its fundamental elements, using particle accelerators and colliders. In the LHC, it is possible not only to collide head on bunches of 10^{11} protons (p) but also heavy ions such as lead nuclei.

The LHC was designed for a $\mathscr{L} = 10^{34}$ cm^{-2}s^{-1} peak of instantaneous luminosity for proton collisions [8]. Figure 2 sketches the operation and upgrade plan of the LHC from 2011 until 2040. At the end of Run 1, $p-p$ collisions at centre-of-mass energy of $\sqrt{s}$ =8 TeV were collected reach-

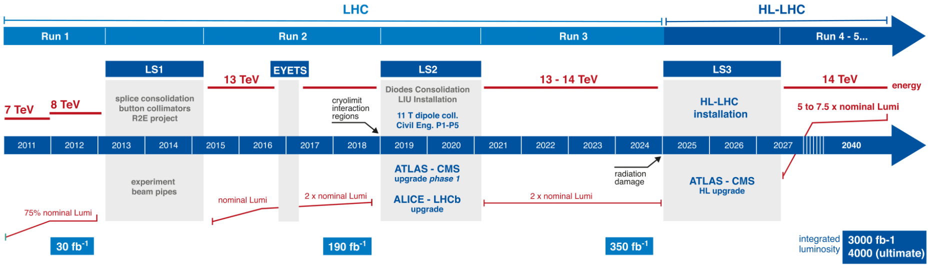

Figure 2. LHC and High Luminosity LHC upgrade plan [7].

ing an integrated luminosity 30 fb^{-1}. During the LHC Run 2, the integrated luminosity between 2015 to 2018 was approximately 150 fb^{-1}, and the nominal luminosity ranged from 5-20 $\times 10^{33}$ cm^{-2}s^{-1} for $p-p$ collisions at $\sqrt{s}=13$ TeV [9]. Run 3 is expected to start, after two years and a half of shut down, at the end of 2021 and during this period the integrated luminosity is expected to be 160 fb^{-1}. According to this plan, in 2027, the HL-LHC phase will start. The instantaneous luminosity is expected to increase 5 to 7.5 × the nominal one so the integrated luminosity can reach more than 3000 fb^{-1}.

A. The ATLAS detector

The ATLAS (A Toroidal LHC ApparatuS) experiment operates at the LHC and is responsible for detecting, measuring, tracking, and identifying the various products of the collision reaction and to investigate a wide range of high energy physics phenomena. The ATLAS detector is divided into four subsystems: the inner detector [10] responsible for reconstructing the trajectories of electrically charged particles produced in the collision, the two calorimeters [11, 12] which measure the energy of electrons, photons and hadrons, and the muon spectrometer [13] that serves to identify and measure muon trajectories with precision and the magnet system [14].

B. The ATLAS Tile Calorimeter

The Tile Calorimeter (TileCal), a hadronic calorimeter, is an essential detector of the ATLAs experiment at the LHC. This sampling detector, located in the ATLAS central region, is made of plastic scintillator tiles as the active medium, interleaved with steel plates as absorbers [15, 16]. The scintillation light produced through the passage of particles reaches the photomultiplier tubes (PMTs) through two wavelength shifting optical fibres connected to each edge of the tile. A TileCal components schematic is presented in Figures 3 and 4. A bundle of fibres groups several tiles into a common readout by a single PMT, defining the detector cell. In total, the Tile calorimeter has 5182 cells each one is readout by two PMTs channels (one from the left and another from the right).

TileCal is divided into three barrels: one Long Barrel (LB) located in $|\eta|$[1] < 1.0 and two Extended Barrels (EB) located on opposite sides of the LB and covering $0.8 < |\eta| < 1.7$. Each is segmented into three radial layers — A, BC and D — and the granularity of the cell, in η and ϕ, is $0.1(0.2)\times 0.1$ for the A and BC(D) layers, as illustrates Figure 3.

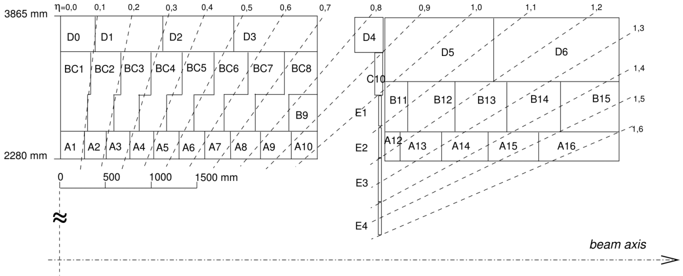

Figure 3. Map of Tiles cells of the LB and EB [15].

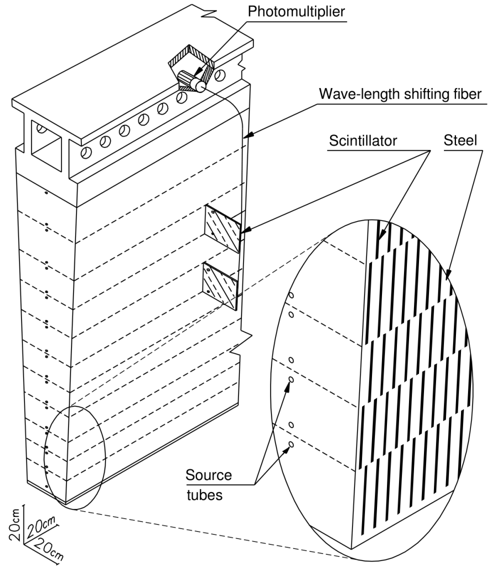

Figure 4. Schematic of the optical readout of the TileCal [15].

---

[1] ATLAS uses a right-handed coordinate system with its origin at the nominal interaction point (IP) in the centre of the detector and the z-axis coinciding with the axis of the beam pipe. The x-axis points from the IP towards the centre of the LHC ring, and the y-axis points upward. Cylindrical coordinates (r,ϕ) are used in the transverse plane, ϕ being the azimuthal angle around the z-axis. The pseudorapidity is defined in terms of the polar angle θ as $\eta = -ln\tan\frac{\theta}{2}$. The distance in (η,ϕ) coordinates, $\Delta R = \sqrt{(\Delta\phi)^2 + (\Delta\eta)^2}$ so used to define cone sizes. Transverse momentum and energy are defined as $p_T = p\sin\theta$ and $E_T = E\sin\theta$, respectively.

C. TileCal Calibration and Monitoring Systems

The TileCal employs three dedicated calibration systems, sketched in Figure 5, to maintain the energy measurement calibrated against fluctuation of the response of any of the readout elements.

Such fluctuations can be due to the high light fluxes that cause instabilities in the PMTs response and light yield degradation of the scintillators with radiation exposure. The cell energy in GeV is reconstructed as:

$$E = A \times C_{pC\rightarrow GeV} \times f_{ADC\rightarrow pC} \times f_{Cs} \times f_{Las} \tag{2}$$

where A is the signal amplitude in ADC counts, $f_{ADC\rightarrow pC}$ is the ADC to pC conversion factor measured by the Charge Injection System (CIS), $C_{pC\rightarrow GeV}$ is the pC to GeV conversion factor defining the detector energy scale, determined with electron beams in past beam tests, and f_{Cs} and f_{Las} are calibration factors extracted from the Cesium and Laser calibrations, respectively [17].

The Cesium source calibration system (Cs) is responsible for calibrating the response of the entire chain: tiles, fibres ans PMTs. The Laser calibration system (Las) calibrates the PMTs and the electronics. The Charge injection system is used to calibrate the electronic readout.

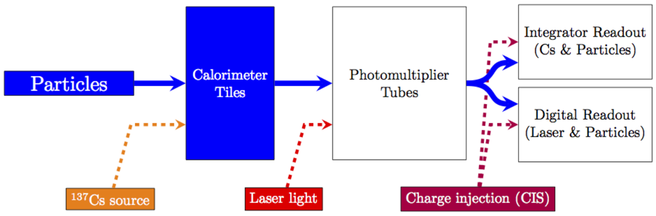

Figure 5. Schematic of the TileCal calibration systems [18].

IV. TileCal Calibration with the Laser System

The uncertainties on the PMT response calibration using the Laser system are usually evaluated making a direct comparison between the calorimeter response to the Cs scans and Laser pulses. This procedure relies on frequent Cs scans where the effects from radiation damage on the optics are small enough to be neglected, i.e., where the evolution of the Cs constants should match the evolution of the Laser constants. Since the Cs system had a leakage problem not enough Cs scans were available for the years 2017 and 2018. A new indirect method was developed to determine the uncertainties on the PMT response, $R(PMT)$, that takes advantage of the double cell readout of TileCal and explores the responses to Cs, $R(Cs)$, and Laser measured with left and right PMTs reading the same cell.

The Cs calibration system provides information about the response of the TileCal optics (scintillator tiles and fibres) ($R(tiles+fibres)$) and the response of the PMTs ($R(PMT)$), and can be factorised into these two components:

$$R(Cs) = R(tiles+fibres) \times R(PMT) \tag{3}$$

Rewriting Equation 3, the optical response read by the left PMT is:

$$R(tiles+fibres_L) = \frac{R_L(Cs)}{R_L(PMT)} \tag{4}$$

and by the right PMT is:

$$R(tile+fibres_R) = \frac{R_R(Cs)}{R_R(PMT)}. \tag{5}$$

where the R and L subscripts denote the response measured through the right and left side channels of the cell, respectively.

Assuming that the difference between the response given by the left and the right fibres connected to the same cell is equal, i.e. assuming $R(fibres_L) = R(fibres_R)$, one can write:

$$R(tile+fibres) = \frac{R_L(Cs)}{R_L(PMT)} = \frac{R_R(Cs)}{R_R(PMT)} \tag{6}$$

and the difference between the measured $\frac{R_L(Cs)}{R_L(PMT)}$ and $\frac{R_R(Cs)}{R_R(PMT)}$ can be explored to determine the uncertainties on the PMT response calibration.

The four Cesium scans and the four closest Laser runs to these scans, taken during the year 2018, were used. There was no Cs scan for one of the LB data used, as a consequence the data for this Barrel has only three scans. The relative response to the Laser system, x^{Las}, is determined with respect to the Laser run close to the reference Cs scan.

The relative response to Cs, x^{Cs}, is determined with respect to the first Cs scan as the reference scan.

The difference between the left and right side measurements of $R(tiles+fibres)$ is defined as:

$$\sigma_1[\%] = \frac{100}{\sqrt{2}}\left(\frac{x_L^{Cs}}{x_L^{Las}} - \frac{x_R^{Cs}}{x_R^{Las}}\right) \tag{7}$$

where the σ_1 value is the standard deviation of the gaussian fit to the distribution of the quantity in the right-hand side of Equation 7 and is around 0.3-0.6% for the EB and LB as shown in Figure 6.

The value of σ_1 has a contribution from the Laser uncertainty and from the Cs uncertainty as well. In order to disentangle their different contributions, the difference between the relative response of the left and right cell readout to the Cs and to the Laser systems were independently analysed using these equations:

$$\sigma_2[\%] = \frac{100}{\sqrt{2}}\left(x_L^{Cs} - x_R^{Cs}\right) \tag{8}$$

$$\sigma_3[\%] = \frac{100}{\sqrt{2}}\left(x_L^{Las} - x_R^{Las}\right) \tag{9}$$

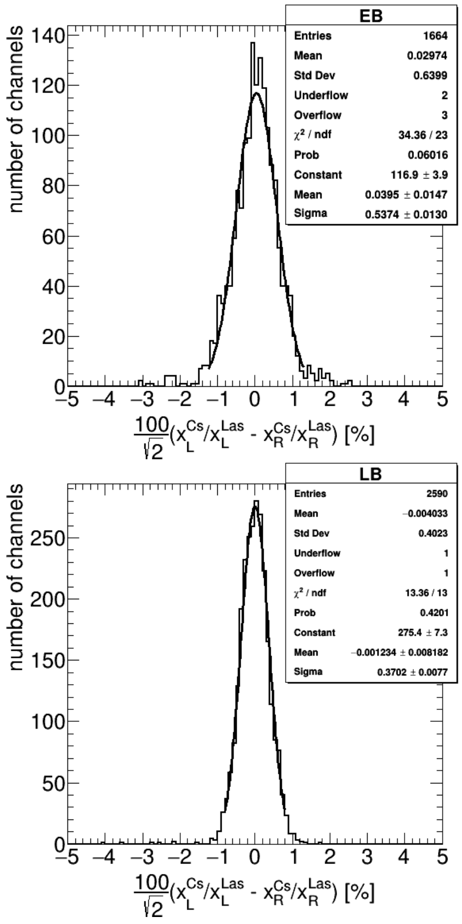

Figure 6. Distribution of the difference between the ratio of the left relative response to Cesium and Laser and the ratio of the right relative response to Cesium and to Laser for (top) the Extended Barrel and (bottom) the Long Barrel. A gaussian function was adjusted to the data, the parameters of the fit are presented in the plot.

by combining information from Equations 7, 8 and 9 it is possible to isolate the σ_{Laser} value. The results obtained for σ_1, σ_2 and σ_3, and σ_{Laser} are plotted as a function of the integrated luminosity and shown in Figure 7. σ_{Laser} increases linearly with the luminosity. Therefore a linear equation was fitted to the σ_{Laser} points to derive a parametrisation of these uncertainties with an explicit luminosity dependence. This was derived separately for the Extended and Long Barrels.

This method computes the intrinsic relative uncertainty on the PMT calibration, but if a systematic error were to shift all the PMT responses by a given amount it would not be captured by it. Previous studies showed that the uncertainty on the Laser calibration global scale is no more than 0.4% [18]. This value is summed in quadrature with the linear fit result in order to obtain the total uncertainty.

So, the final uncertainties on the PMT response to the Laser system as a function of the integrated luminosity, L, for the EB, σ^{EB}_{Laser}, and LB, σ^{LB}_{Laser}, separately are:

$$\sigma^{EB}_{Laser} = 0.5 + 0.2/63.3 \times L \tag{10}$$

$$\sigma^{LB}_{Laser} = 0.5 + 0.1/63.3 \times L \tag{11}$$

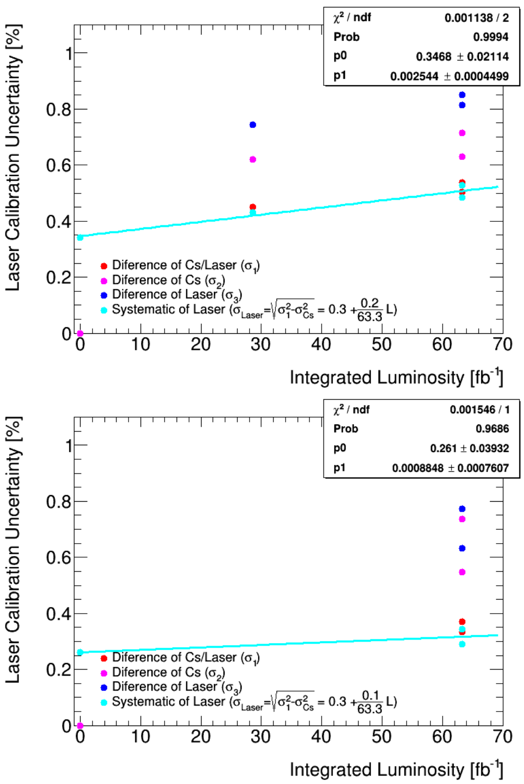

Figure 7. The standard deviations σ_1, σ_2, σ_3, and σ_{Laser} as a function of the integrated luminosity for the (top) Extended Barrel and (bottom) Long Barrel. A linear equation was fitted to the σ_{Laser} points. The fit result is shown in the plot.

The study of the uncertainties on the response to the Laser system was an essential input to study the degradation of the optical components.

V. Radiation hardness of the Tile Calorimeter optical components

The current LHC plans foresee a Run 3 and a HL-LHC phase, and will extend the TileCal lifetime further from the design goals. Since the optical components cannot be replaced, their radiation damage must be studied.

The deviation of the cells' response to the Cs (ΔR_{Cs}) and to the Laser (ΔR_{Las}) during the Run 2 are presented in Figures 8 and 9. At the end of this Run, the response to the Cs for the A layer had reduced by about 10% and the response of the PMTs to the Laser, for the same layer, had reduced by about 4%. The difference between the cell's response to the Cs and the PMT's response to the Laser corresponds to a variation of the response of the scintillators and fibres, interpreted as degradation due to radiation. Therefore, by subtracting the two responses, we can isolate the optical response. We define the relative light yield (I/I_0) of the cell's scintillators and fibres as:

$$I/I_0 = 1 + \frac{\Delta R_{Cs} - \Delta R_{Las}}{100\%}. \quad (12)$$

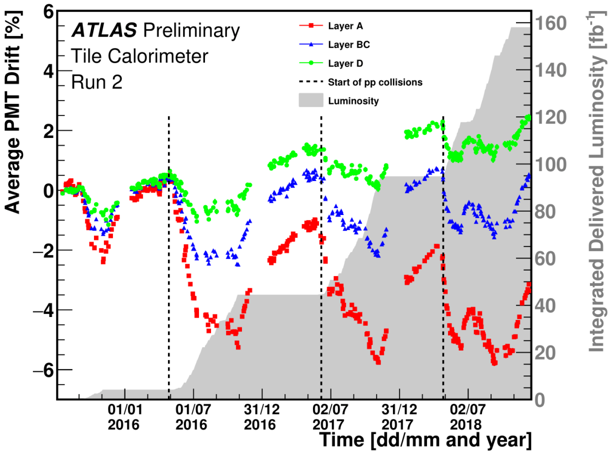

Figure 8. Evolution of the mean relative response of the 3 longitudinal layers (A, BC, D) in the ATLAS Tile Calorimeter as a function of time, as measured by the Laser calibration system. The dashed lines indicate the start of the pp collisions period in the respective years. The LHC delivered luminosity is shown for comparison [19].

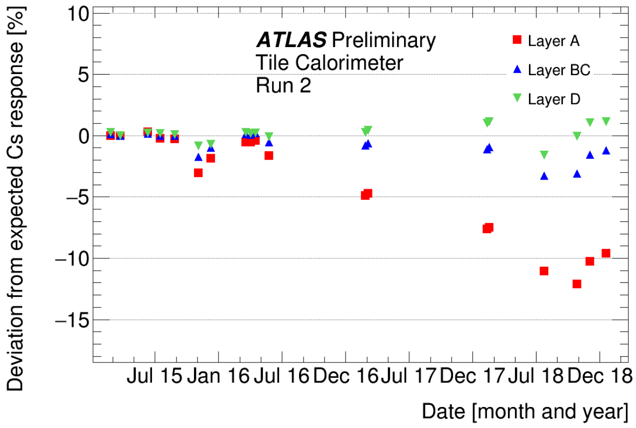

Figure 9. Evolution of Tile Calorimeter response to Cesium source as a function of time in 3 different longitudinal layers [20].

Figure 10 shows that the relative light yield decreases with the increase of the dose, obtained with GEANT4 simulation of the ATLAS detector in the TileCal region for 50000 $p-p$ generated collisions at the centre-of-mass energy of $\sqrt{s} = 13$ TeV [21]. The dose was simulated in bins of 4 cm $\times$ 4 cm in the $z \times r$ plan. The Total Ionisation Doses in a given cell is obtained by multiplying the integrated luminosity by the dose conversion factor for the cell. For instance, the dose for the A13 cell for an integrated luminosity of 158.1 fb^{-1} (end of Run 2) is 67 Gy. The average cell dose conversion factors for Run 2 are shown in Figure 11, the A layer is the most exposed one since they are closer to the beam pipe.

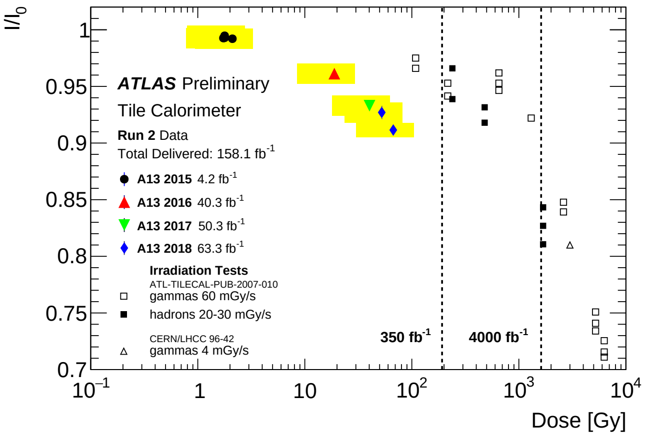

Figure 10. The measured relative light yield for the A13 cell as a function of the simulated dose in Run 2. The vertical errors are associated to the precision of the Cs and Laser systems, and the horizontal band corresponds to the dose spread within the large cell volume. The square markers are data from bare scintillators irradiated before the calorimeter construction [22].

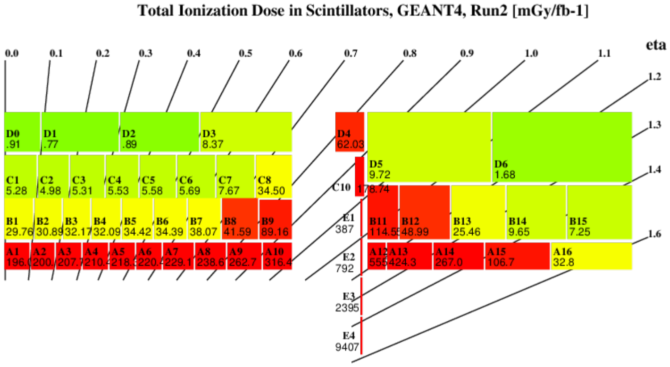

Figure 11. Average ionisation dose conversion factor per TileCal cell determined using GEANT4 simulation of the ATLAS detector in the Tile calorimeter region for 50000 $p-p$ generated collisions at the centre-of-mass energy of $\sqrt{s} = 13$ TeV. The ATLAS detector was simulated with geometry corresponding to the Run 2 operation.

The relative light yield was mapped for the end of Run 2 and is represented in Figure 13. The cells more exposed to radiation are the cells in the A layer, and B11 and C10 cells. They have a light yield loss of the order of 5%. For the other cells no degradation is observed. The relative uncertainty is of the order of 1%.

The relative light yield measurement was extrapolated to the end of Run 3, by fitting the Run 2 data with a simple exponential function (Figure 14):

$$I/I_0 = e^{(p_0 - dose/p_1)}. \quad (13)$$

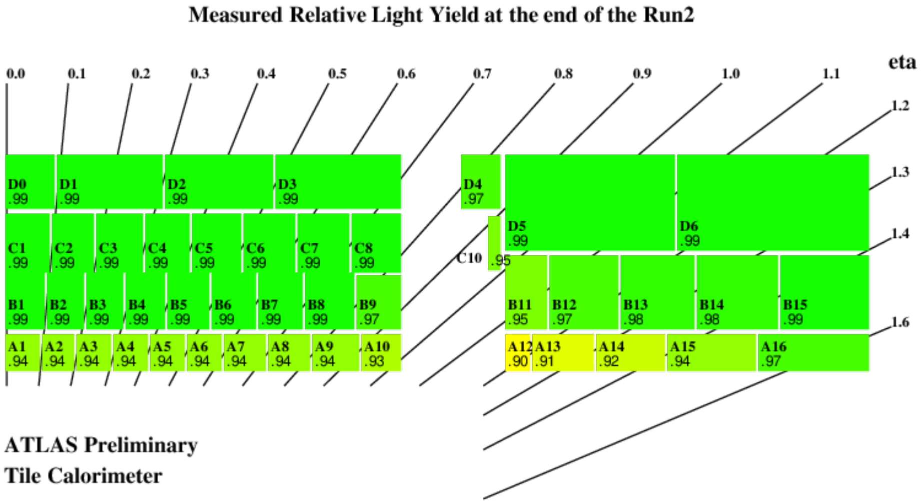

Figure 13. The measured relative light yield of the TileCal cells at the end of Run 2 [22, 23]

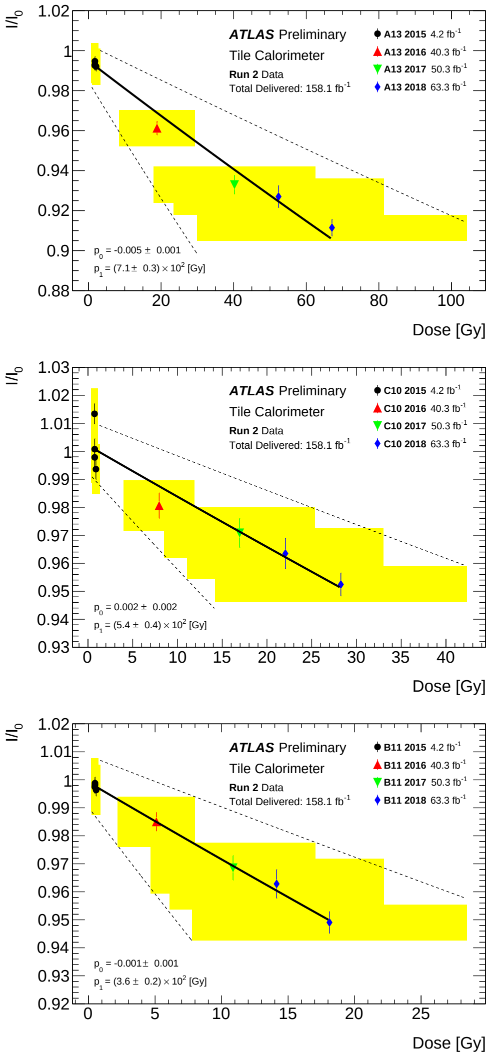

Figure 14. The relative light yield for the A13, B11 and C10 cell as a function of the simulated dose during the LHC Run 2 [18].

The results show that the more affected cells are in layer A, and cells B11 and C10 with an expected loss between 6 and 21%. For the remaining cells the expected loss is between 1 and 6% (Figure 15 top). The relative uncertainty on the extrapolation is of the order of 5%.

Since this model does not take into account a possible recovery or additional degradation of the scintillators between LHC runs, the end of Run 3 is also the beginning of the HL-LHC, so it is expected for TileCal to enter the HL-LHC phase with most of the cells unaffected in terms of the light response. Preliminary results extrapolating to the end of the HL-LHC, in Figure 15 bottom show that the most affected cells are again in layer A, and B11 and C10 cells, with an expected loss of light yield between 59 and 90%. For the remaining BC and D4 cells, the expected loss is between 25 and 50%. For the cells in the D layer, the expected loss is between 12 and 29%. The relative uncertainty on the extrapolation ranges from 40 to 100% for cells in the A layer, B11 and B12 cells, and is around 10% for the remaining ones. The uncertainties are very large, so it is still premature to make final conclusions about the TileCal radiation damage at the end of the HL-LHC. More data from Run 3 will be needed to have more precision in the extrapolation.

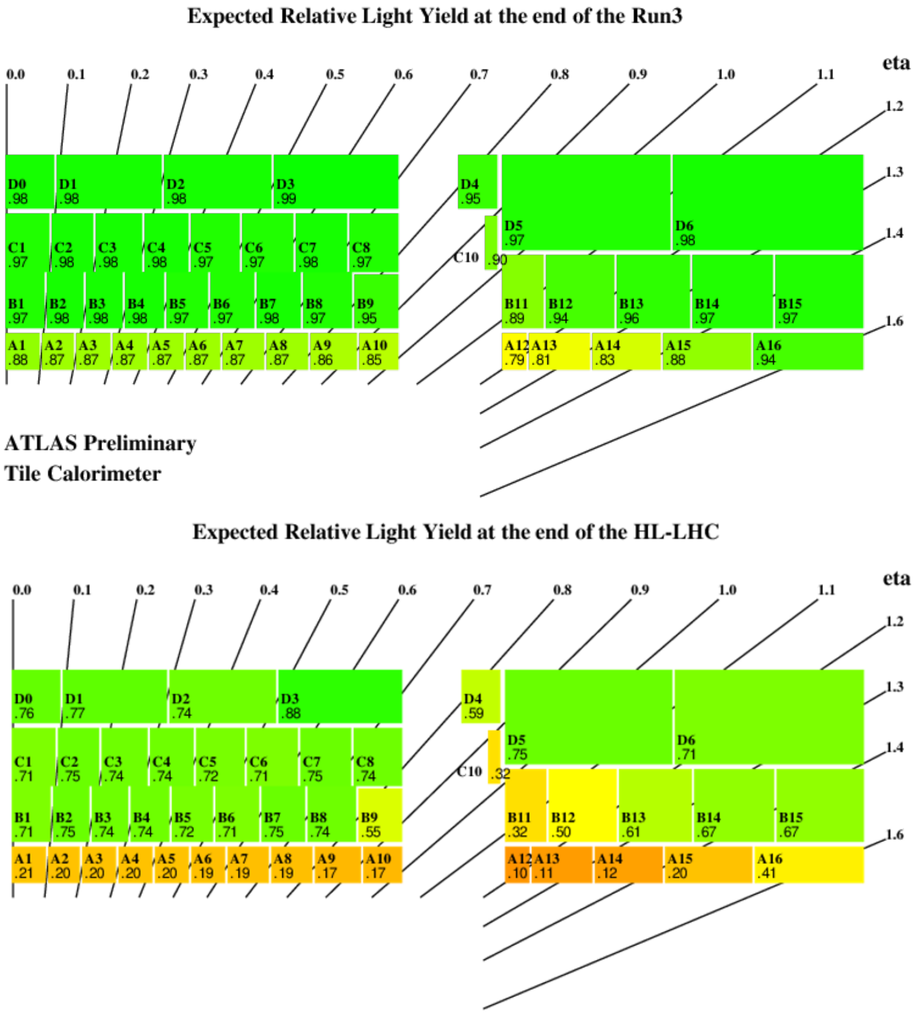

Figure 15. Expected relative light yield of the TileCal cells at the (top) end of Run 3 and at the (bottom) end of HL, assuming an integrated luminosity of 350 fb^{-1} and 4000 fb^{-1}, respectively.

Previous studies have shown that the degradation not only depends on the absorbed dose but also on the dose rate, indicating that for smaller dose rate values, the degradation would occur more rapidly. In the simple exponential model, the larger the p_1 value the smaller the degradation rate, for it means that more dose must be accumulated to reach 37% light yield degradation. To study the possible impact of the dose rate effects, the fit parameter p_1 is plotted as a function of the dose conversion factors in Gy/fb^{-1} for the most degraded cells in Figure 16. The dose conversion factors are a good proxy for dose rate since they are directly proportional to each other: in order to obtain the dose rate, one just needs to multiply the dose conversion factor, in Gy/fb^{-1}, by the instantaneous luminosity at the LHC, in fb^{-1}/s. The results show that p_1 increases with dose rate, and so, the degradation rate decreases with the dose rate. Taking into account the large uncertainties, the conclusions are less clear. Nevertheless, if the uncertainties on the p_1 values have a purely systematic nature, we could conclude that the dose rate has an impact on the degradation of the scintillators.

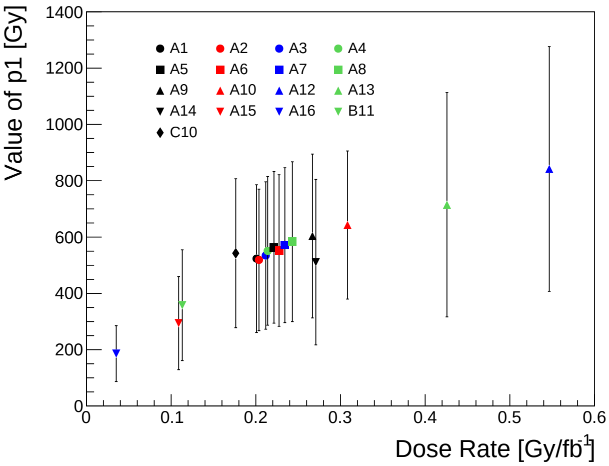

Figure 16. Value of p_1 parameter, obtained by an exponential fit of the form $e^{p_0 - dose/p_1}$ for the most degraded cells as a function of the dose rate in Gy/fb^{-1}.

VI. Conclusions

The main work of this thesis consisted of studying the radiation hardness of the optical components of the ATLAS Tile Calorimeter. These components can degrade with radiation exposure compromising TileCal performance. Since the detector's lifetime will be extended, it is mandatory to study what can be expected during the future years in order to design mitigation strategies if needed. The strategies and the knowledge learned during the radiation hardness study can be broadened to future colliders.

The analysis is based on the difference in the calorimeter response to the Cesium and the Laser calibration systems. The uncertainties on the PMT calibration are addressed by a comparison between the TileCal response to the Cesium and Laser calibration systems using 2018 data. The final uncertainty obtained has a constant term around 0.5% and a term dependent on the integrated luminosity that reaches 0.1% at 63.3 fb^{-1} integrated luminosity in 2018.

The uncertainties on the PMT calibration were used in the evaluation of the radiation hardness of the TileCal optical components. The relative light yield of the detector cell's scintillators and fibres in Run 2 was measured using Cesium and Laser calibration data. The innermost cells are the most affected ones, which is expected since they are closer to the LHC beam pipe and the dose deposit is larger. Measurements during this Run have shown that cells in layer A, and B11 and C10 cells have already lost about 5% of light yield. Within 1% of uncertainty, no significant changes were found for the other cells.

A simple exponential was used to model the light yield degradation as a function of the accumulated dose simulated with GEANT4 for each TileCal cell. The parameters of the fit are different from cell to cell, indicating that they will degrade at different rates. One factor that may contribute to this is the dose rate.

The light yield degradation was extrapolated to the end of the Run 3 and High Luminosity LHC phase from the exponential fit to the Run 2 measurements. At the end of Run 3, the great majority of TileCal cell is not expected to degrade more than 2 to 6%, while the most exposed cells belonging to the layer A, and the B9 and C10 cells expects a light loss between 6 and 21%. The extrapolation uncertainty is about 5%. The preliminary results from the extrapolation to the end of the HL-LHC phase show a light loss between 50 and 12% for most of the BC and all the D layers, with a relative uncertainty of 10%. A significant light loss is shown for the A layer cells, but the uncertainties are very large and possible effects of recovery during long shut down periods were not taken into account.

Part of the future work is to use more data, from the Run 3, to reduce the extrapolation uncertainty on the relative light yield at the end of the HL-LHC phase and to evaluate the impact of the relative light loss in the detection of particles. It is also important to study, in more detail, the dose rate impact in the degradation process and at which values this phenomenon is more substantial as well as study and to model the recovery of the scintillator materials.

Acknowledgements

Thanks are due to Dr. Rute Pedro and Prof. Patricia Muino for all the help during the development of this project.

[1] "2020 update of the european strategyfor particle physics by the european strategy group." `https://home.cern/sites/home.web.cern.ch/files/2020-06/2020%20Update%20European%20Strategy.pdf`. Accessed: 2020-10-13.

[2] Y. N. Kharzheev, "Radiation hardness of scintillation detectors based on organic plastic scintillators and optical fibers," *Physics of Particles and Nuclei*, vol. 50, no. 1, pp. 42–76, 2019.

[3] Y. Sirois and R. Wigmans, "Effects of long-term low-level exposure to radiation as observed in acrylic scintillator: Cause and prevention of radiation disease in uranium calorimeters," *Nuclear Instruments and Methods in Physics Research Section A: Accelerators, Spectrometers, Detectors and Associated Equipment*, vol. 240, no. 2, pp. 262–274, 1985.

[4] A. Collaboration, "The production and qualification of scintillator tiles for the atlas hadronic calorimeter," tech. rep., 2007.

[5] W. R. Leo, *Techniques for nuclear and particle physics experiments: a how-to approach*. Springer Science & Business Media, 2012.

[6] V. Khachatryan, A. Sirunyan, A. Tumasyan, A. Litomin, V. Mossolov, N. Shumeiko, M. Van De Klundert, H. Van Haevermaet, P. Van Mechelen, A. Van Spilbeeck, *et al.*, "Dose rate effects in the radiation damage of the plastic scintillators of the cms hadron endcap calorimeter," *Journal of Instrumentation*, vol. 11, no. 10, p. T10004, 2016.

[7] "Image of the lhc high luminosity upgrade." `https://project-hl-lhc-industry.web.cern.ch/sites/project-hl-lhc-industry.web.cern.ch/files/inline-images/HL-LHC-plan-2020-Plan-1.pdf`. Accessed: 2020-07-22.

[8] L. Evans and P. Bryant, "Lhc machine," *Journal of instrumentation*, vol. 3, no. 08, p. S08001, 2008.

[9] "Lhc report: The final days of run 2." `https://home.cern/news/news/accelerators/lhc-report-final-days-run-2`. Accessed: 2020-07-17.

[10] A. Collaboration, "Atlas inner detector : Technical design report, 1." `https://cds.cern.ch/record/331063`.

[11] A. Collaboration, "Atlas liquid-argon calorimeter : Technical design report." `https://cds.cern.ch/record/331061`.

[12] A. Collaboration, "Atlas tile calorimeter : Technical design report, cern-lhcc-96-042," tech. rep., 1996.

[13] A. Collaboration, "Atlas muon spectrometer : Technical design report." `https://cds.cern.ch/record/331068`.

[14] A. Collaboration, "Atlas magnet system : Technical design report, 1." `https://cds.cern.ch/record/338080`.

[15] A. Collaboration, "Technical design report for the phase-ii upgrade of the atlas tile calorimeter," tech. rep., 2017.

[16] A. Collaboration, "The atlas experiment at the cern large hadron collider," *Jinst*, vol. 3, p. S08003, 2008.

[17] P. Klimek and on behalf of the ATLAS Collaboration, “Calibration and performance of the atlas tile calorimeter during the lhc run 2,” in *Journal of Physics: Conference Series*, vol. 1162, p. 012003, IOP Publishing, 2019.

[18] “Calibration public plots.” `https://twiki.cern.ch/twiki/bin/view/AtlasPublic/ApprovedPlotsTileCalibration`. Accessed: 2020-09-30.

[19] “Evolution of the mean relative response measured by the laser calibration system.” `https://twiki.cern.ch/twiki/bin/view/AtlasPublic/ApprovedPlotsTileCalibrationLaser`. Accessed: 2020-08-26.

[20] “Evolution of tile calorimeter response to cesium source.” `https://twiki.cern.ch/twiki/bin/view/AtlasPublic/ApprovedPlotsTileCalibration#Cesium`. Accessed: 2020-08-26.

[21] “Radiation public plots.” `https://twiki.cern.ch/twiki/bin/view/AtlasPublic/RadiationSimulationPublicResults`. Accessed: 2020-10-25.

[22] “Light yield public plots.” `https://twiki.cern.ch/twiki/bin/view/AtlasPublic/ApprovedPlotsTileCalibrationCombined`. Accessed: 2020-11-05.

[23] B. o. b. o. t. A. C. Pereira, “Radiation hardness of the atlas tile calorimeter optical components,” in *Journal of Physics: Conference Series*, vol. 1690, p. 012053, IOP Publishing, 2020.